Stochastic Resonance-Enhanced Radio Frequency Fingerprinting Under Low-SNR Conditions

Youli Guo*

Shanghai Key Laboratory of Naviation and Location Baseed Services, Shanghai 200030, China

*Corresponding author's e-mail: youliguo0530@gmail.com

Abstract. Radio frequency fingerprinting (RFF) faces significant challenges under low signal-to-noise ratio conditions where conventional denoising methods suppress device-specific features. We propose a stochastic resonance (SR)-based enhancement framework that decomposes complex signals into the in-phase (I) and quadrature (Q) components and processes them through optimized bistable SR systems. Evaluation on ten transmitters across signal-to-noise ratio (SNR) range of 0 to -20 dB shows our approach achieves medium-to-large effect sizes compared to conventional denoising methods in majority conditions, demonstrating improved identification performance in extreme low-SNR environments.

Keywords. Radio Frequency Fingerprinting, Stochastic Resonance, Machine Learning, Deep Learning

1. Introduction

RFF has emerged as a critical technology for device authentication in wireless networks, leveraging inevitable hardware imperfections during RF transmission to distinguish transmitters [1]. Recent advances in lightweight edge AI, attention-based feature fusion, and Siamese architectures have enabled high-accuracy RFF on resource-constrained devices [2,3,4], while transient and time-frequency features have proven effective for capturing hardware "fingerprints" under realistic channel conditions [5]. However, reliable recognition in low-SNR environments remains a challenge that device fingerprints become submerged in noise, causing sharp performance degradation [6,7]. Traditional approaches follow two strategies: enhanced denoising to recover cleaner signals [8], or designing noise-robust features and classifiers [2,3,4].

Departing from conventional noise suppression paradigms, this work explores SR. The idea is that appropriate noise levels can induce resonance in nonlinear systems, amplifying weak signals beyond linear SNR limits [9,10]. SR has demonstrated promise in sensing, acoustics, fault diagnosis, and communications for weak-signal enhancement [11,12,13]. Early energy detection studies showed parameter-induced SR can reduce SNR thresholds [9], while recent theoretical work provides insights on noise-assisted sensing in nonlinear systems [10]. This paper investigates bistable SR as a preprocessing mechanism for RFF identification. We process I/Q signal components through parameterized bistable SR systems, optimizing it via cross-correlation maximization with clean references during training. Evaluation across SNR ranges from 0 to -20 dB using signals from ten transmitters demonstrates SR's effectiveness against conventional denoising baselines including Wiener filtering (WF), spectral subtraction (SS), and discrete wavelet transform (DWT). The main contributions are: (1) a dual-channel SR framework that exploits noise to enhance RF fingerprints via separate I/Q component processing; (2) a data-driven constrained optimization strategy that automatically configures the SR system by maximizing cross-correlation with pristine reference suitable for supervised learning; (3) comprehensive validations down to -20 dB SNR, showing superior performance over classical denoising methods in majority conditions with statistically significant improvements.

2. Methodology

2.1. Signal Modelling

We begin by modelling the pristine transmitted signal in complex exponential form:

$$s(t) = A(t)e^{j(2\pi f_c t + \phi(t))} \tag{1}$$

where $s(t)$ represents the ideal modulated signal generated at the transmitter, $A(t)$ is the time-varying amplitude containing the baseband information, f_c is the carrier frequency, and $\phi(t)$ represents the phase modulation. For the Quadrature Amplitude Modulation considered in this work, $\phi(t)$ is defined in the principal range of $(-\pi, \pi]$. The signal experiences channel distortions and additive noise during transmission, resulting in the received signal:

$$r(t) = s(t) + n(t) \tag{2}$$

where $n(t)$ encompasses all noise contributions including thermal noise, phase noise, and interference. Usually, the real part is defined as I and the imaginary part is defined as Q. Thus, the received signal can be converted into a dual-channel real-valued representation

$$r_{I/Q} = \begin{bmatrix} r_I(t) \\ r_Q(t) \end{bmatrix}, r_{I/Q} \in \mathbb{R}^{2\times N} \tag{3}$$

where N represents the number of samples in our observation window. This dual-channel representation preserves both amplitude and phase information while facilitating subsequent processing in the SR framework.

2.2. Non-linear Bistable SR System

Considering the bipolar nature of r_I and r_Q, we employ a bistable SR system characterized by a double-well potential function independently on both I and Q channels of the received signal. The system dynamics are governed by the Langevin equation:

$$\frac{d\tilde{x}}{dt} = -\frac{dU(\tilde{x})}{d\tilde{x}} = a\tilde{x} - b\tilde{x}^3 + \tilde{r}(t) \tag{4}$$

where $(\sim)$ denotes any one side of the dual channel, $\tilde{x}$ represents the enhanced signal or internal state, whose potential function is defined as:

$$U(\tilde{x}) = \frac{b}{4}\tilde{x}^4 - \frac{a}{2}\tilde{x}^2 - \tilde{r}\tilde{x} \tag{5}$$

For $a > 0$, $b > 0$, and $r = 0$, the potential trail exhibits two stable equilibria at $x = \pm\sqrt{a/b}$ separated by an unstable equilibrium at $x = 0$. The barrier height between the wells is $\Delta U = \frac{a^2}{4b}$, which determines the system's sensitivity to noise-induced transitions. The received signal $r(t)$ now serves as an external forcing term that breaks the symmetry of the double well potential, creating a time-varying bias that facilitates directional transitions between the stable states. When $r(t) > 0$, the potential tilts to favor the right-hand stable equilibrium, thereby increasing the probability of transitions into that state. Conversely, when $r(t) < 0$, the bias favors the left-hand equilibrium, promoting transitions in the opposite direction. The stronger the bias is, the more pronounced the directional tendency of the state transition.

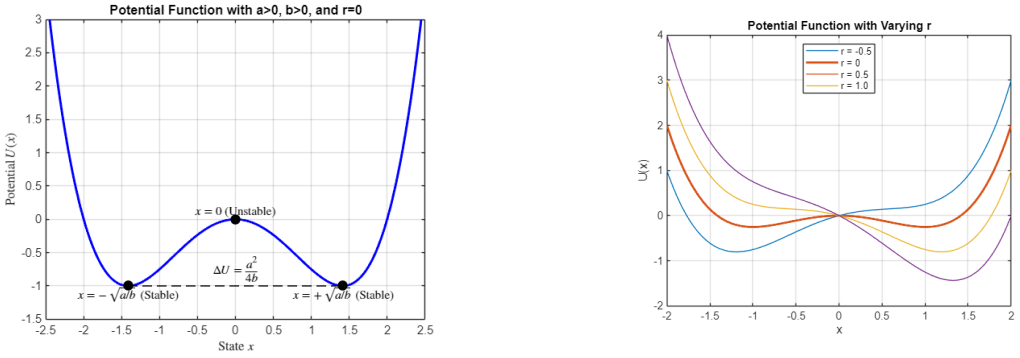

Figure 1. Motion Trajectories of Bistable Systems.

Previous studies have shown that SR becomes effective when the noise intensity is suitably matched to the potential barrier height $\Delta U(a,b)$ relative to the characteristic timescales of the weak input signal [14]. While theory suggests optimal SR occurs through direct control of $\Delta U(a,b)$, our data-driven approach described in Section 2.3 (equation 9) maximizes cross-correlation with pristine signals, implicitly seeking parameter combinations $\{a,b\}$ that optimize enhancement performance.

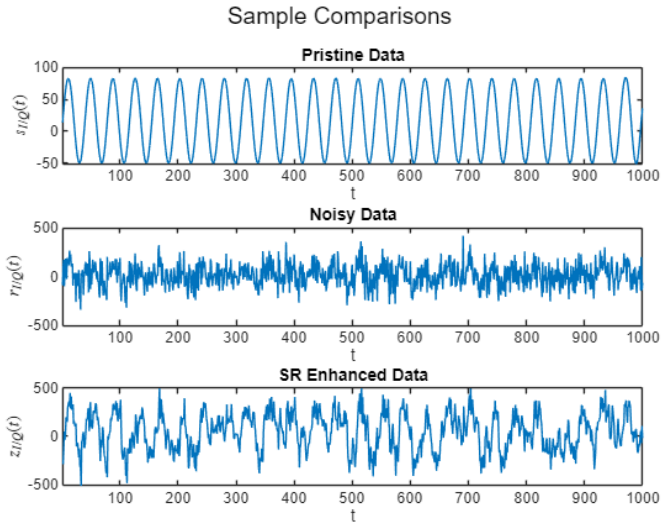

Figure 2. Signal Comparisons with SNR = -10.

2.3. System Parameter Optimization

The effectiveness of the SR system critically depends on the proper selection of system parameters a, b, and the integration time step. To ensure numerical stability and facilitate parameter optimization, we first apply a normalization transformation to the SR system. Starting from equation (4), we introduce scaling factors θ and γ such that $\tau = \theta t$ and $\tilde{z} = \gamma \tilde{x}$. By the chain rule:

$$\frac{d\tilde{z}}{d\tau} = \frac{a}{\theta}\tilde{z} - \frac{b}{\gamma^2\theta}\tilde{z}^3 + \frac{\gamma}{\theta}\tilde{r} \tag{6}$$

Setting $\gamma = \sqrt{\frac{b}{a}}$ and $\theta = 1$, then $\frac{a}{\theta} = \frac{b}{\gamma^2\theta} = 1$, resulting in the normalized form:

$$\frac{d\tilde{z}}{d\tau} = \tilde{z} - \tilde{z}^3 + \sqrt{\frac{b}{a^3}}\tilde{r} \tag{7}$$

For discrete-time implementation, we discretize equation (7) using the Euler method:

$$\tilde{z}[n+1] = \tilde{z}[n] + \left(\tilde{z}[n] - \tilde{z}^3[n] + \sqrt{\frac{b}{a^3}}\,\tilde{r}[n]\right)d\tau \tag{8}$$

where $d\tau$ represents the integration time step that controls the system's temporal resolution and stability. The optimization objective is formulated to maximize the modulus of the cross-correlation between SR-enhanced signals and their pristine counterparts:

$$\rho = arg\,\max_{a,b,d\tau} \frac{1}{M}\sum_m^M \left| \frac{\sum_n^N \left(z^{(m)}[n] - \bar{z}^{(m)}\right)\left(s^{(m)}[n] - \bar{s}^{(m)}\right)^*}{\sqrt{\sum_n^N \left|z^{(m)}[n] - \bar{z}^{(m)}\right|^2 \sum_n^N \left|s^{(m)}[n] - \bar{s}^{(m)}\right|^2}} \right| \tag{9}$$

where M is the number of samples, $(-)$ denotes the mean of one sample, $(*)$ denotes complex conjugation, $(\,||\,)$ denotes complex modulus, and $z^{(m)}[n] = z_I^{(m)}[n] + jz_Q^{(m)}[n]$. $\{a,b,d\tau\}$ are constrained within empirical bounds to ensure system stability and prevent numerical overflow [9], and we solve such constrained optimization problem via MATLAB's *fmincon* function with interior-point algorithm. This preprocessing optimization is feasible under supervised learning settings by restricting parameter optimization to the training set (where pristine references are assumed available), avoiding

data leakage while maintaining generalizability to testing data (where only corrupted signals are present to simulate realistic deployment scenarios).

3. Experimental Evaluation

This section presents a two-stage experimental design focused on wireless signal classification that serves dual purposes: identifying the optimal classifier for the task and eliminating potential bias from selectively choosing a classifier that might artificially favour our proposed SR enhancement method. First, we identify the most effective classifier from a range of machine learning algorithms under various low SNR conditions. Second, using the top-performing classifier, we compare the enhancement efficacy of our SR method against several established denoising techniques to validate the advantages of leveraging SR in noisy environments. The experiments are conducted using a wireless signal dataset provided by the *Shanghai Key Laboratory of Navigation and Location-Based Services*, which includes signals from ten distinct transmitters with 1400 noise-free complex-valued array samples per class, each containing 4000 I/Q sampling points. Inter-class variations arise solely from hardware-specific differences among transmitters.

3.1. Signal Processing and Classifiers Setups

Starting with the original pristine signals from distinct emitters, we introduce several levels of additive white Gaussian noise (AWGN) to simulate realistic channel impairments, ranging from 0 dB to -20 dB in 2 dB decrements. For each SNR level, the noisy dataset is randomly partitioned using stratified sampling to maintain the balanced distribution, with 80% allocated to the training set and the remainder to the test set. The data split is performed independently for each noise level to ensure unbiased evaluation across different SNR conditions. Crucially, SR parameter optimization leverages the pristine references corresponding to the training set samples, while the test set samples have no access to their pristine counterparts, simulating realistic deployment scenarios.

We utilize the training data in conjunction with their pristine counterparts to optimize the SR system according to the framework described in Section 2, with initial stage $z_{I/Q}[1] = \bar{r}_{I/Q}$ and bounds set to ensure numerical stability according to empirical ranges [9]: $a \in [0.001, 100]$, $b \in [0.001, 100]$, and $d\tau \in \left[\frac{1}{3000}, \frac{1}{1000}\right]$. The optimal parameters $\{a, b, d\tau\}$ are applied to both the training and testing datasets, yielding their enhanced versions while preserving the original data partitioning structure.

We also include several baseline methods for comparison, including WF, SS, and DWT [8]. To ensure fairness, the training and testing partitions are fixed in advance and remain identical across all methods; the parameters of each enhancement model are derived from the training set and subsequently applied to both training and testing sets. Specifically, for DWT, we use soft thresholding with Bayesian shrinkage rule, where parameters are optimized via grid search over wavelet types $\{db1, db2, db4, haar\}$ and decomposition levels {4,5,6,7,8}.

We implement three traditional classifiers: Gaussian support vector machine (GSVM), decisions tree (DT), and k-nearest neighbors (KNN). All three traditional classifiers undergo Bayesian optimization with 5-fold cross-validation to ensure robust parameter selection. All classifiers consistently achieve convergence within 30 iterations under such settings. We also design a CNN for dual-channel I and Q inputs of size $4000 \times 2 \times 1$. The network consists of three convolutional blocks. Each block applies a two-dimensional convolution with a 3×1 kernel along the temporal axis, followed by batch normalization and a rectified linear unit activation. The first two blocks additionally include a 2×1 max-pooling layer with stride 2×1. The numbers of filters in the three blocks are 32, 64, and 128, respectively. After the final block, a global average pooling layer reduces the representation to a 128-dimensional embedding. The classifier consists of a fully connected layer with 64 units and rectified linear activation, a dropout layer with probability 0.5, and a final fully connected layer with 10 units and softmax activation. The network is trained using the Adam optimizer with an initial learning rate of 0.001, mini-batch size of 32, and a maximum of 100 epochs, incorporating a step-wise learning rate decay and validation on a held-out test set.

3.2. Experiment Results

We first demonstrate that CNN is the most effective classifier across the considered low-SNR conditions. We conducted classification experiments at each SNR level using all candidate classifiers on both non-enhanced and enhanced signals (processed by WF, SS, DWT, and SR). For each classifier, the result from the best-performing condition is selected to represent its performance at that SNR, thereby objectively reflecting the classifier's maximum potential under noise. Traditional classifiers (GSVM, KNN, and DT) were evaluated over 30 independent runs and CNN results were averaged over 5 runs, with SR and DWT parameters re-optimized for each individual run in both cases. The resulting accuracy values and standard deviations are summarized in Table 1. The highest accuracy at each SNR level is highlighted in bold, and cases where SR yields the best enhancement result for a particular classifier are additionally underlined.

Table 1. Classifier Comparisons (Average Accuracies).

SNR (dB)	Tree	GSVM	KNN	CNN
0	0.2286±2.1×10^{-3}	0.5504±5.3×10^{-3}	0.9371±3.7×10^{-3}	**0.9582**±8.2×10^{-3}
-2	0.1925±1.8×10^{-3}	0.4261±4.6×10^{-3}	0.8961±6.4×10^{-3}	**0.9475**±9.1×10^{-3}
-4	0.1714±3.2×10^{-3}	0.3039±7.8×10^{-3}	0.8489±5.5×10^{-3}	**0.9271**±7.3×10^{-3}
-6	0.1593±2.4×10^{-3}	0.1964±3.1×10^{-3}	0.7664±8.9×10^{-3}	**0.8500**±6.7×10^{-3}
-8	0.1446±1.5×10^{-3}	0.1543±2.8×10^{-3}	0.6493±4.2×10^{-3}	**0.7372**±7.4×10^{-3}
-10	0.1404±1.3×10^{-3}	0.1321±2.2×10^{-3}	0.5232±7.6×10^{-3}	**0.6161**±8.8×10^{-3}
-12	0.1239±1.6×10^{-3}	0.1207±1.4×10^{-3}	0.4339±6.1×10^{-3}	**0.4954**±9.5×10^{-3}
-14	0.1257±1.2×10^{-3}	0.1104±1.9×10^{-3}	0.3396±3.8×10^{-3}	**0.3925**±4.7×10^{-3}
-16	0.1057±8×10^{-5}	0.1086±5×10^{-5}	0.2396±2.3×10^{-3}	**0.2989**±6.2×10^{-3}
-18	0.1000±4×10^{-5}	0.1000±3×10^{-5}	0.1632±4.5×10^{-3}	**0.2096**±5.1×10^{-3}
-20	0.1000±2×10^{-5}	0.1000±2×10^{-5}	0.1400±3.4×10^{-3}	**0.1536**±2.9×10^{-3}

Since the samples are perfectly balanced, accuracy is representative of overall performance. As shown in Table 1, CNN consistently achieves the highest classification accuracy across all SNR levels. Moreover, the Welch's t-test results for CNN versus the second-best performing classifier (KNN) shown in Table 2 demonstrate statistically significant superiority of CNN across all SNR levels, with all $p < 0.001$ except for SNR = 0 dB where $p < 0.01$.

Table 2. One-sided Welch's t-test (CNN vs KNN).

SNR (dB)	CNN	KNN	Improvement (%)	t-values	p-values
0	0.9582	0.9371	2.25	5.659	1.97×10^{-3}
-2	0.9475	0.8961	5.74	12.140	5.11×10^{-5}
-4	0.9271	0.8489	9.21	22.895	2.23×10^{-6}
-6	0.8500	0.7664	10.91	24.526	4.77×10^{-8}
-8	0.7372	0.6493	13.54	25.875	2.58×10^{-6}
-10	0.6161	0.5232	17.76	22.263	1.56×10^{-6}
-12	0.4954	0.4339	14.17	14.002	3.17×10^{-5}
-14	0.3925	0.3396	15.58	23.899	1.42×10^{-6}
-16	0.2989	0.2396	24.75	21.146	1.03×10^{-5}
-18	0.2096	0.1632	28.43	19.140	3.05×10^{-6}
-20	0.1536	0.1400	9.71	9.459	3.98×10^{-5}

Therefore, subsequent analyses of enhancement methods are based on the CNN results. As observed from Table 3, SR-enhanced signals achieve the best accuracy performance across most SNR conditions, but with notable exceptions at SNR = -8 and -10 dB, where WF demonstrates superior performance.

Table 3. Enhancement Comparisons (Average Accuracies, under CNN).

SNR (dB)	Raw	SR	WF	SS	DWT
0	0.8986	**0.9582**	0.9429	0.8521	0.8957
-2	0.8332	**0.9475**	0.9429	0.8054	0.8321
-4	0.6932	**0.9271**	0.9043	0.7221	0.7157
-6	0.5689	**0.8500**	0.8393	0.6211	0.4736
-8	0.4671	0.7350	**0.7372**	0.5064	0.2971
-10	0.3604	0.6150	**0.6161**	0.3650	0.2129
-12	0.2636	**0.4954**	0.4850	0.2389	0.1621
-14	0.1661	**0.3925**	0.3896	0.1504	0.1293
-16	0.1275	**0.2989**	0.2936	0.1264	0.1068
-18	0.1093	**0.2096**	0.2075	0.1068	0.1157
-20	0.1071	**0.1536**	0.1479	0.1000	0.1000

We report metrics consisting accuracy and macro F1-score and perform Cohen's d test respectively to further demonstrate the effectiveness of SR over WF.

Table 4. Cohen's d test (SR vs WF, on Accuracies).

SNR (dB)	SR	WF	Improvement (%)	d Score
0	**0.9582**$\pm 8.2\times10^{-3}$	$0.9429\pm 7.5\times10^{-3}$	+1.62	+1.947
-2	**0.9475**$\pm 9.1\times10^{-3}$	$0.9422\pm 7.1\times10^{-3}$	+0.56	+0.649
-4	**0.9271**$\pm 7.3\times10^{-3}$	$0.9043\pm 6.0\times10^{-3}$	+2.52	+3.412
-6	**0.8500**$\pm 6.7\times10^{-3}$	$0.8393\pm 5.2\times10^{-3}$	+1.28	+1.784
-8	$0.7350\pm 8.7\times10^{-3}$	**0.7372**$\pm 7.4\times10^{-3}$	-0.30	-0.272
-10	$0.6150\pm 5.6\times10^{-3}$	**0.6161**$\pm 8.8\times10^{-3}$	-0.18	-0.149
-12	**0.4954**$\pm 9.5\times10^{-3}$	$0.4850\pm 7.6\times10^{-3}$	+2.14	+1.209
-14	**0.3925**$\pm 4.7\times10^{-3}$	$0.3886\pm 7.3\times10^{-3}$	+0.74	+0.579
-16	**0.2989**$\pm 6.2\times10^{-3}$	$0.2936\pm 9.5\times10^{-3}$	+1.80	+0.661
-18	**0.2096**$\pm 5.1\times10^{-3}$	$0.2075\pm 4.5\times10^{-3}$	+1.01	+0.437
-20	**0.1536**$\pm 2.9\times10^{-3}$	$0.1479\pm 2.4\times10^{-3}$	+3.85	+2.141

Table 4. Cohen's d test (SR vs WF, on Macro F-1).

SNR (dB)	SR	WF	Improvement (%)	d Score
0	**0.9582**$\pm 8.0\times10^{-3}$	$0.9430\pm 6.9\times10^{-3}$	+1.61	+2.035
-2	**0.9481**$\pm 8.8\times10^{-3}$	$0.9427\pm 7.4\times10^{-3}$	+0.57	+0.664
-4	**0.9282**$\pm 7.7\times10^{-3}$	$0.9056\pm 6.8\times10^{-3}$	+2.49	+3.111
-6	**0.8520**$\pm 6.2\times10^{-3}$	$0.8396\pm 5.1\times10^{-3}$	+1.48	+2.184
-8	$0.7390\pm 7.9\times10^{-3}$	**0.7413**$\pm 7.8\times10^{-3}$	-0.31	−0.293
-10	$0.6127\pm 6.3\times10^{-3}$	**0.6132**$\pm 8.1\times10^{-3}$	-0.08	−0.069
-12	**0.4810**$\pm 9.2\times10^{-3}$	$0.4693\pm 7.3\times10^{-3}$	+2.49	+1.409
-14	**0.3753**$\pm 4.5\times10^{-3}$	$0.3716\pm 7.9\times10^{-3}$	+1.00	+0.576
-16	**0.2924**$\pm 6.5\times10^{-3}$	$0.2875\pm 9.2\times10^{-3}$	+1.70	+0.615
-18	**0.2020**$\pm 5.1\times10^{-3}$	$0.1984\pm 4.3\times10^{-3}$	+1.81	+0.763
-20	**0.1527**$\pm 3.2\times10^{-3}$	$0.1469\pm 2.6\times10^{-3}$	+3.95	+1.989

The Cohen's d test results in Tables 4 and 5 provide compelling evidence for the superior performance of the proposed SR-based enhancement approach. Across both accuracy and macro F1-score metrics,

SR demonstrates improvements over the WF baseline in the majority of SNR conditions. While WF marginally outperforms SR at SNR = -8 and -10 dB, these advantages are minimal with $|d| < 0.3$, suggesting negligible practical significance. In contrast, when SR outperforms WF, the improvements are consistently more substantial, with Cohen's d scores all larger than 0.5 and frequently exceeding 1.0, indicating medium to large practical effect sizes. This asymmetric pattern underscores the general superiority of the SR-based approach, where its advantages are meaningful while its occasional disadvantages are marginal, establishing its effectiveness as a preprocessing technique.

4. Conclusion and Future Works

This study presented a novel application of a SR-based framework for enhancing corrupted wireless signals, specifically targeting the challenge of RFF under low-SNR conditions. By formulating system parameter optimization as a constrained correlation-maximization problem and implementing them on I and Q components, the proposed SR framework yields statistically significant improvements over classical denoising techniques across most scenarios, providing a robust preprocessing solution that leverages noise constructively to enhance discriminative features, rather than merely suppressing it. Despite promising results, the approach has two main limitations: (1) SR parameters were optimized independently of classifier training; (2) insufficient cross-scenario generalization validation with single data source with balanced samples and controlled conditions. Future work will explore embedding SR modules into end-to-end trainable networks and using self-supervised and evaluating cross-receiver, cross-channel, and open-set generalization performance with unbalanced samples.

References

[1] Zhang H, Zhou F, Du H, Wu Q and Yuen C (2025) Revolution of Wireless Signal Recognition for 6G: Recent Advances, Challenges and Future Directions. *arXiv preprint*, arXiv:2503.08091.

[2] Hussain A M, Abughanam N and Papadimitratos P (2024) Edge AI-based Radio Frequency Fingerprinting for IoT Networks. *arXiv preprint*, arXiv:2412.10553.

[3] Zeng Y, Gong Y and Liu J et al. (2023) Multi-Channel Attentive Feature Fusion for Radio Frequency Fingerprinting. *IEEE TWC (preprint on arXiv)*, arXiv:2303.10691.

[4] Dhakal R, Kandel L N and Shekhar P (2024) Radio Frequency Fingerprinting Authentication for IoT Networks Using Siamese Networks. *Journal of Internet of Things* (MDPI), 6(3):47.

[5] Ahmed N et al. (2025) Enhancing Wireless Device Identification through RF Fingerprinting: Leveraging Transient Energy Spectrum Analysis. *arXiv preprint*, arXiv:2506.17439.

[6] Jiang Q and Sha J (2024) RF Fingerprinting Identification in Low SNR Scenarios for Automatic Identification System. *IEEE Transactions on Wireless Communications*, 23: 2070–2081.

[7] Lacy F, Ruiz-Reyes A and Brescia A (2024) Machine Learning for Low Signal-to-Noise Ratio Detection. *Pattern Recognition Letters*, 2024.

[8] Yousif S T and Mahmmod B M (2025) Speech Enhancement Algorithms: A Systematic Literature Review. *Algorithms* (MDPI), 18(5):272.

[9] Liu J and Li Z (2015) Lowering the signal-to-noise ratio wall for energy detection using parameter-induced stochastic resonator. *IET Communications*, 9(1):101–107.

[10] Ho J S, et al. (2023) Stochastic Exceptional Points for Noise-Assisted Sensing. *Physical Review Letters*, 130:227201.

[11] Wang Y, Li Y, Wang L, Lu Y and Zhou Z (2025) A Novel Hyperbolic Unsaturated Bistable Stochastic Resonance System and Its Application in Weak Signal Detection. *Applied Sciences*, 15(16):8970.

[12] Zhang C, Lai Z, Tu Z and Liu H (2024) Stochastic resonance induced weak signal enhancement in a second-order tri-stable system with single-parameter adjusting. *Applied Acoustics*, 216:109753.

[13] Liu G and Wang D (2024) Study of the characteristics of second-order underdamped unsaturated stochastic resonance system driven by OFDM signals. *Applied Sciences*, 14(23):11324.

[14] Gammaitoni L, Hänggi P, Jung P and Marchesoni F (1998) Stochastic resonance. *Reviews of Modern Physics*, 70(1):223–287.